Quenching effects in organic electrophosphorescence

J. Kalinowski, W. Stampor, and J. Mężyk
Department of Molecular Physics, Technical University of Gdańsk, ul. G. Narutowicza 11/12, 80-952 Gdańsk, Poland

M. Cocchi, D. Virgili, V. Fattori, and P. Di Marco
Institute of Organic Synthesis and Photoreactivity, National Research Council of Italy, via P. Gobetti 101, 40129 Bologna, Italy

(Received 3 April 2002; revised 30 July 2002; published 31 December 2002)

We examine various electronic processes that underlie the quenching of the emission from highly efficient phosphorescent and electrophosphorescent organic solid-state molecular systems. As an example, we study the luminescent efficiencies from the phosphorescent iridium (III) complex, *fac* tris (2-phenylpyridine) iridium $[\mathrm{Ir}(ppy)_3]$ doped into a diamine derivative doped polycarbonate hole-transporting matrix and in the form of vacuum-evaporated films, as a function of electric field. We demonstrate that the observed decrease in electrophosphorescence efficiencies at high electric fields, and electric-field-induced quenching of phosphorescence from neat $[\mathrm{Ir}(ppy)_3]$ solid films is due to the field-assisted dissociation of Coulombically correlated electron-hole (*e*-*h*) pairs. They are formed in a bimolecular recombination process prior to the formation of emissive triplet excitons, or are charge-transfer (CT) states originating from the localized electronic excited states as a result of the initial charge separation upon photoexcitation, respectively. It is found that the high-field dependence of the quenching efficiency in both cases follows the three-dimensional Onsager theory of geminate recombination, the fit yielding the initial intercarrier distance (r_0) of the carrier pairs. We find $r_{e\text{-}h} \geqslant 3.5$ nm for the triplet exciton precursor pairs in the bimolecular recombination, and $r_{\mathrm{CT}} = 1.8 \pm 0.1$ nm for the initial carrier separation from the photo-excited electronic states. Triplet-triplet and triplet-charge carrier annihilation processes are shown to play major roles in the decrease of the electrophosphorescence efficiency within the lower-field regime at lower current densities. Summarizing the results allows us to point out some emitter features important for identifying phosphors useful for practical electroluminescent devices.

DOI: 10.1103/PhysRevB.66.235321 PACS number(s): 78.66.Qn, 78.60.Fi, 72.20.My

I. INTRODUCTION

Organic electrophosphorescence (EPH) is a form of electroluminescence (EL) where the optical emission originates from triplet excitons relaxing radiatively to the singlet ground electronic state (S_0), due to their quantum mechanical mixing with singlet states. In organic EL, excited states are created by applying an electric field to a liquid or a solid state specimen made of an organic compound. Different types of organic EL can be distinguished based on the excitation mode of emitting states. These are (i) high-field EL with excited states produced by direct electron tunneling from the valence band or an acceptor state to the conduction band; (ii) impact EL, occurring as a result of a field-accelerated electron impact with host molecules or dopant luminescent centers; and (iii) recombination EL, where excited states are produced in a bimolecular electron-hole (*e*-*h*) recombination process. EL types (i) and (ii), observed mostly in inorganic semiconductors, were also considered to underlie the optical emission in early works on organic EL. The present efforts are focused on understanding and applications of the recombination EL, perhaps the most common type of EL occurring in organics (a more detailed description of organic EL can be found in Ref. 1).

The formation of localized emitting species in the recombination process of the injected positive and negative charges implies a natural intermediate step of Coulombically correlated charge pairs (CP's) which have undefined spin character being a mixture of singlet and triplet states characterized by antiparallel ($\uparrow\downarrow$, $\downarrow\uparrow$) and parallel ($\uparrow\uparrow$, $\downarrow\downarrow$) carrier spins, respectively (see Fig. 1). The singlet-to-triplet amplitude ratio of their states is often assumed to be 1:3 by spin statistics arguments, supported partly by an experimental study of the archetype EL material, aluminum *tris* (8-hydroxyquinoline)

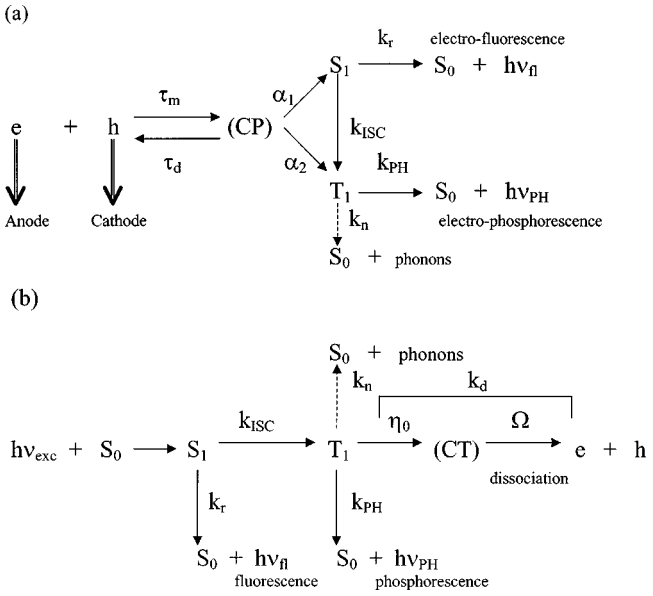

FIG. 1. Formation of molecular excited states (S_1,T_1) and charge pair states [(CP) and (CT)] in the course of bimolecular electron-hole recombination (a) and under optical excitation (b). For a phosphorescent material the radiative decay of singlets (k_r) is negligible, the system exhibits only phosphorescence and electrophosphorescence.

(Alq_3).[2] However, recent experimental[3–5] and theoretical[6] works provided support for previous suggestions that the singlet-to-triplet state outcome ratio can be completely different.[7] This is a consequence of carrier trapping and the spin-dependent formation cross section of excited states. If one of the recombining carriers is trapped at a depth $\Delta E > E_g - E_S$ (where E_g is the energy gap and E_S is the singlet exciton energy), the energetics of the process must be taken into account,[8] the recombination probability to form a singlet state can be expressed as $\alpha_1 = (1/4)\exp\{-[\Delta E - (E_g - E_S)]/kT\}$, the probability of the formation of a triplet is then $\alpha_2 = 1 - \alpha_1$. It is obvious that for deep traps and/or small $E_g - E_S$, $\alpha_1 \ll 1/4$ and $\alpha_2 \to 1$. The branching ratio α_1/α_2 for the CP states does not translate directly to the singlet/triplet spin occupation ratio of the final emitting states because each of the CP states is a superposition of the overall eigenstate of the initial reactant species and the overall eigenstate of the final products of the recombination reaction. The outcome of the recombination reaction is thus dominated by the ionic character of the initial species; favoring the creation of correlated singlet excitons revealing a remarkable ionic character, whereas the correlated triplet excitons have a large covalent character. Since, in turn, the ionicities are correlated with the overall optical gap, one would expect the singlet-to-triplet outcome ratio to be strongly material dependent as, in fact, was recently observed in π-conjugated polymers.[5] For the above reasons, resulting formation rates (α_1, α_2) appear to be, in general, a complex function of material properties including their chemical nature and sample morphology. In spite of this, in an overwhelming majority of organic materials, the α_1/α_2 ratio does not seem to overcome $\frac{1}{3}$, and the spin-forbidden radiative decay of triplet excitons is very inefficient ($k_{PH} \ll k_n$ in Fig. 1). This means that in most cases we deal with electrofluorescence, the majority of excited triplet states is lost for the emission, limiting the EL efficiency. Triplet excitons can be gained over to radiative processes using a phosphorescent material[9–12] and/or a fluorescent dye excited in an energy-transfer process from the phosphorescent triplets.[13] A nearly 20% external EL quantum efficiency was reached in organic light emitting devices employing phosphorescent molecules doped into a wide energy-gap host.[14,15] However, the overall EPH output does not increase in a simple proportion to the current flowing through the samples since the EPH quantum efficiency has been found to decrease by more than one order of magnitude at high current densities.[9,16] This is a serious shortcoming of electrophosphorescent light-emitting diodes, and a detailed knowledge of the emission quenching is required in order to improve their performance.

The observed quenching of the EPH output was explained by triplet-triplet (*T*-*T*) exciton annihilation, a process that becomes very efficient at a high concentration of triplet excitons produced under high-current density conditions.[16] Since the exciton concentration is proportional to the intrinsic exciton lifetime, one would expect the quenching effect for long-living triplets to exceed that for short lifetime singlet excitons, whereas the observed high-current density drop in the electrofluorescent light-emitting diodes is comparable[17–22] to that for electrophosphorescent systems.

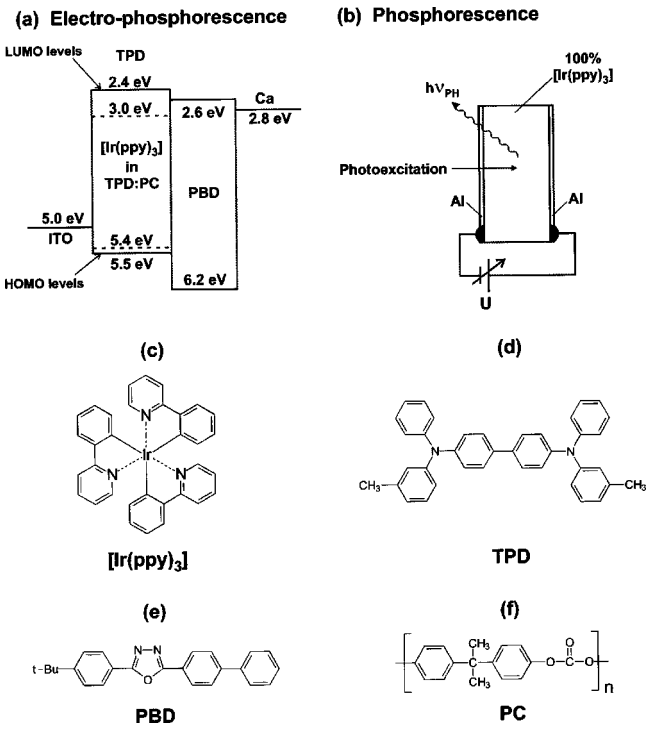

FIG. 2. Schematic representations of the electrophosphorescent system (a) and the sandwich configuration used to measure electric field-induced phosphorescence quenching (b). The molecular structures of the materials used: (c) $[Ir(ppy)_3]$ fac tris (2-phenylpyridine) iridium, (d) TPD (N,N'-diphenyl-N,N'-bis(3-methylphenyl)-[1,1′-biphenyl]-4,4′-diamine, (e) PBD 2-(biphenyl-4-yl)-5-(4-tert-butylphenyl)-1,3,4-oxadiazole, and (f) PC bisphenol-A-polycarbonate.

Thus exciton-exciton annihilation alone cannot explain the observed exciton quenching phenomena. Exciton-charge carrier interaction and electric field-assisted dissociation of excitons (or their CP precursors) are conceivable exciton quenching mechanisms, as already discussed for the case of electro-fluorescence[22] and electric-field-induced quenching of fluorescence[23,24] from organic solids.

Here we study electric-field-induced triplet exciton quenching effects using the phosphor *fac* tris-(2-phenylpyridine) iridium $[Ir(ppy)_3]$ either as an emitter in a highly efficient EPH device or as a neat solid sample prepared by a thermal vacuum evaporation technique. We outline a theoretical basis for triplet-triplet, triplet-charge carrier, and triplet exciton dissociation phenomena applied to explain the present and other existing already experimental results. Furthermore, we discuss discrepancies between various experimental data and the theoretical predictions, before concluding.

II. EXPERIMENT

The electrically and optically excited structures are shown in Fig. 2. The EPH properties of $[Ir(ppy)_3]$ were studied in thin film devices of which the device ITO/6% wt$[Ir(ppy)_3]$: 74 wt% TPD:20 wt% PC(50 nm)/100% PBD (50 nm)/ Ca/Ag revealed the highest EPH quantum efficiency and pro-

vided the most useful data for comparison with theory. The phosphorescent iridium complex [Ir(ppy)$_3$] [*fac* tris(2-phenyl-pyridine) iridium] was synthesized, identified and purified as described in the literature,[25,26] PBD [2-(biphenyl-4-yl)-5-(4-tert-butylphenyl)-1,3,4-oxadiazole] and TPD [*N*,*N*′-diphenyl-*N*,*N*′-bis(3-methylphenyl-(1,1′-biphenyl)-4,4′-diamine] were purchased from Aldrich, and PC [bisphenol-A-polycarbonate] of mw 32000–36000 from Polysciences Inc. The three latter compounds were used as supplied. Double-layer devices were prepared by a combined spin-coating and vacuum-evaporation techniques. The first layer was spun coat from a 10mg/ml dichloromethane solution onto patterned precleaned transparent to visible light indium-tin-oxide (ITO) coated glass substrates (20 Ω/sq), then the second layer of PBD deposited by vacuum evaporation. The sandwich devices were completed by a vacuum-deposited Ca covered with a protecting layer of Ag. Typically, the active device areas were about 7 mm^2. Chosen spin-coating conditions (2000 rpm) led to 50–60-nm-thick [Ir(ppy)$_3$]:TPD:PC films followed by a similar thickness vacuum-evaporated layer of PBD. The ionization potential of the materials used, represented by the position of the highest occupied molecular orbital (HOMO), makes the ITO anode a good hole injecting contact to the TPD:PC mixture hole-transporting layer (HTL). Their electron affinities, represented by the lowest unoccupied molecular orbital (LUMO) level, enable the Ca cathode to be an efficient injector of electrons and PBD an electron-transporting layer (ETL). The LUMO and HOMO levels of the [Ir(ppy)$_3$] were obtained from the oxidation $E^{\mathrm{ox}}=0.74$ eV potential determined by cyclic voltammetry using the saturated calomel reference electrode in dichloromethane and the optical energy gap resulted from the optical absorption spectrum. The LUMO and HOMO positions of TPD and PBD as referenced to vacuum resulted from the ionization potential of each material[27,28] and the HOMO-LUMO gap identified with the optical energy gap as determined from absorption spectra. Of the materials used, PC is an electronically neutral compound serving as a binding matrix for electrically and optically active molecules of [Ir(ppy)$_3$] and TPD. The electron-hole recombination occurs predominantly at the {[Ir(ppy)$_3$]:TPD:PC}/PBD junction since a wide-gap PBD forms a strong hole blocker. Its removal makes the device much less efficient because of the hole current leakage to the cathode (cf. Secs. III B and III C). TPD and PBD are essentially fluorescent,[29] TPD showing a weak phosphorescence especially at low temperature.[30] To our knowledge no phosphorescence was reported from PBD. As already mentioned, [Ir(ppy)$_3$] is a phosphor which emits at about 510 nm (cf. Sec. III A) with a phosphorescent lifetime of 400 ns.[11,30] The external EPH quantum efficiency, $\varphi_{\mathrm{EPH}}^{(\mathrm{ext})}$, has been determined from the total flux per unit area (I_r in W/cm^2) received by the 1-cm^2 area of an EG&G power meter positioned at a distance $r_M=5$ cm from the devices with forward emitting area $A=7$ mm^2 and the average photon energy ($h\nu$), accounted for the current density j (A/cm^2). Such a light source-detector configuration allowed the light emitting devices to be treated as point radiators with the total radiant flux per unit area, $I_e=(2\pi r_M^2/\mathrm{A})I_r$ (W/cm^2). Thus $\varphi_{\mathrm{EPH}}^{(\mathrm{ext})}=(2\pi r_M^2/A)(I_r/(h\nu))/(j/e)$ (photon/electron).

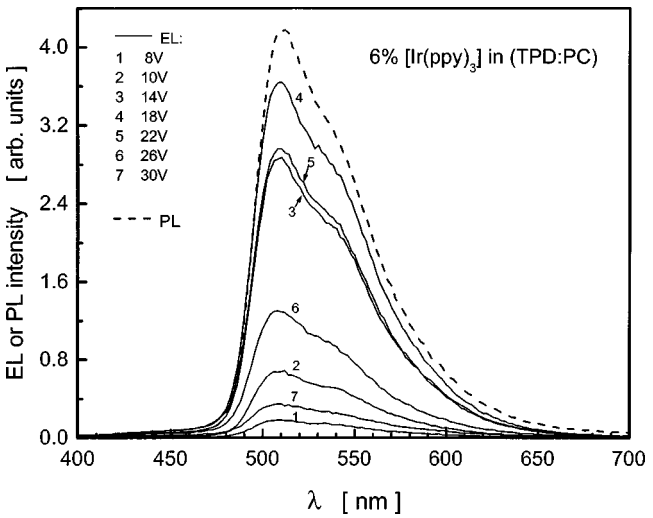

FIG. 3. The spectra of the electrophosphorescent (EPH) device ITO/6%[Ir(ppy)$_3$]:74%TPD: 20% PC (50 nm)/100% PBD (50 nm)/Ca/Ag [cf. Fig. 2(a)], taken at different voltages, (given in the Figure), to be compared with the photoluminescence (PL) spectrum of a thin film of the same composition. Both EPH and PL spectra show a peak at $\lambda\cong 510$ nm and a shoulder at $\lambda\cong 540$ nm characteristic of [Ir(ppy)$_3$]. No emission from TPD: PC matrix and PBD ETL is observed.

The electric-field effect on the [Ir(ppy)$_3$] phosphorescence was measured using typically 0.2-μm-thick vacuum-evaporated films sandwiched between two semitransparent Al electrodes [Fig. 2(b)]. The phosphorescence quenching efficiency was calculated from the difference between phosphorescence signals without and with a dc voltage (U) applied to such sandwich structures. The phosphorescent light was viewed perpendicular to the sample surface. The spectral characteristics of the materials and devices under study were measured with a Perkin Lambda 19UV/Vis/NIR spectrometer and a Spex Fluorolog 2 spectrofluorimeter. The current-voltage characteristics were measured with a Keithley Source-Measure Unit model 236 under continuous operation mode. All EL measurements were conducted in an argon atmosphere, electric-field phosphorescence quenching experiments were performed in air and at room temperature.

III. RESULTS

In this section optical and electrical characteristics of the devices described in Sec. II are reported.

A. Spectral characteristics

The EL spectra of the electrophosphorescent device from Fig. 2(a), taken at various voltages at room temperature, are presented in Fig. 3. Their shape does not change with the applied voltage and corresponds well to the PL spectrum of a [Ir(ppy)$_3$]:TPD:PC layer. This indicates that the final *e-h* recombination emissive products are identical with the

photo-excited emissive states which are supposed to be molecular triplet excitons of $[\mathrm{Ir}(ppy)_3]$ since no fluorescence from TPD, peaking at about 400 nm (see, e.g., Ref. 7), was observed. There are two ways of their generation:

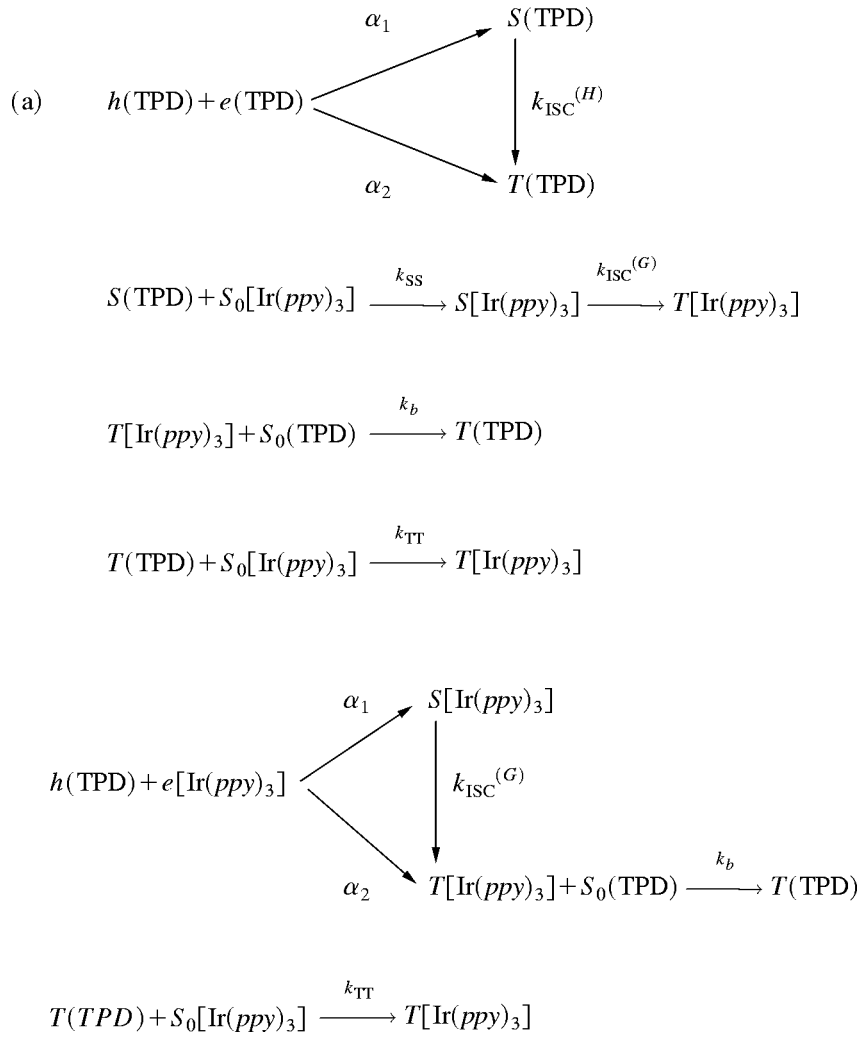

Several processes determine the overall production efficiency of the emissive $[\mathrm{Ir}(ppy)_3]$ triplets in the reaction sequence (a): the probability (α_2) of the formation of the host (TPD) triplets in the bimolecular *e-h* recombination reaction, the rate (k_{SS}) of the long-range (Förster type) singlet-singlet energy transfer from the host (*H*) TPD to guest (*G*) $[\mathrm{Ir}(ppy)_3]$ molecule, the rates of singlet-triplet inter-system crossing transitions for host $[k_{ISC}^{(H)}]$ and guest $[k_{ISC}^{(G)}]$ molecules, and the short-range (Dexter type) host-guest (k_{TT}) and guest-host (k_b) triplet energy transfer. The absence of the fluorescence ($\cong$400 nm) from TPD suggests that the Förster energy transfer rate (k_{SS}) exceeds the radiative decay rate from excited singlets of TPD. If the only source of the guest triplet excitons were the intersystem crossing from the guest singlets populated by the Förster energy transfer from the host matrix, the electro-phosphorescence quantum efficiency would fall in the 1% photon/electron range typical for electrofluorescence underlain by the low values of α_1/α_2 spin branching ratio.[20,22,31] Since the EPH quantum efficiency of the present device (see Sec. III B) exceeds by an order of magnitude that for typical electro-fluorescent devices, one would expect additional efficient channels for generation of the phosphorescent guest triplets. This could be the host-guest triplet energy transfer and/or reaction (b). Indeed, long-time living triplets of the TPD host have been shown to transfer their energy to the phosphorescent guest molecules of $[\mathrm{Ir}(ppy)_3]$.[16] Though this transfer process is impeded by the unfavorable interrelation between the donor and acceptor triplet energies $\{E_T(\mathrm{TPD}) \cong 2.3\ \mathrm{eV} < E_T[\mathrm{Ir}(ppy)_3] \cong 2.4\ \mathrm{eV}\}$, it modifies the guest triplet lifetime to a great extent[30] (also see Sec. IV A). An alternative process of the production of the electro-phosphorescing triplets by reaction (b) still involves the triplet energy exchange between host and guest molecules.

These conclusions are supported by the emission spectrum of an EPH device, where the separated HTL and $[\mathrm{Ir}(ppy)_3]$ layers form a junction alleviating electron injection into and recombination on hole-transporting TPD molecules. It shows up as a field-increasing blue component of its EL spectra presented in Fig. 4. Because increasing voltage applied to the device reduces the energy barrier for electron injection from the $[\mathrm{Ir}(ppy)_3]$ layer, both the concentration of electrons and their penetration depth into the HTL lead to the enhanced *e-h* recombination on hole-transporting molecules of TPD and formation of their emissive singlet excited states. Yet the violet fluorescence from these states ($\cong$400 nm) is very weak since, due to the narrowness of the recombination zone, singlet exciton energy transfer to the $[\mathrm{Ir}(ppy)_3]$ layer is strongly competitive to their radiative decay. The major spectral feature is the maximum at about 515 nm corresponding to the radiative decay of triplet excitons generated by the electron-hole recombination within the layer of $[\mathrm{Ir}(ppy)_3]$. The relative increase of the violet fluorescence component upon removal of the hole blocking layer of PBD indicates a decrease in the EPH emission due to an increased leakage of holes through the $[\mathrm{Ir}(ppy)_3]$ ETL [Fig. 4(b)].

There is an alternative for processes (a) and (b):

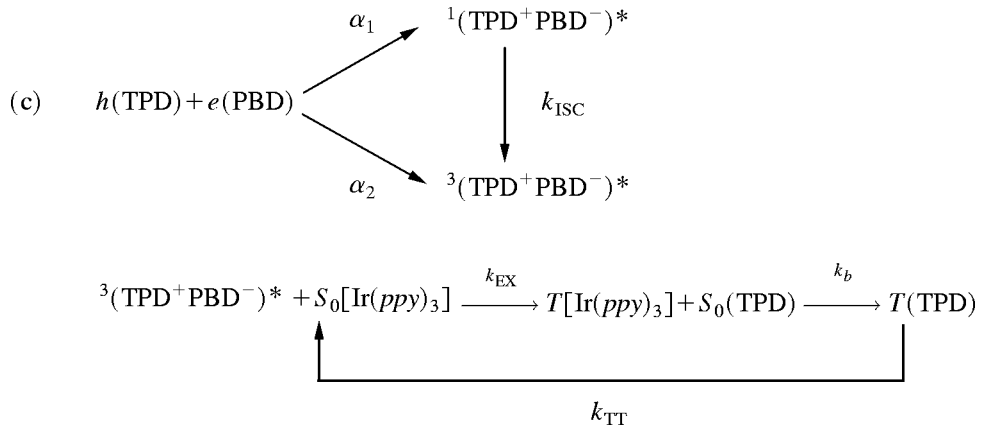

This would invoke a rapid formation of singlet $[^1(\mathrm{TPD}^+\mathrm{PBD}^-)^*]$ and triplet $[^3(\mathrm{TPD}^+\mathrm{PBD}^-)^*]$ exciplexes at the $[\mathrm{TPDIr}(ppy)_3{:}\mathrm{PC}]/\mathrm{PBD}$ interface, the intersystem crossing conversion of the former into their triplet counterparts, and then exciplex energy transfer to the molecularly dispersed $[\mathrm{Ir}(ppy)_3]$. The triplet energy exchange between molecules of $\mathrm{Ir}(ppy)_3$ and TPD (with different rates k_b and k_{TT}) is still expected to affect the resulting concentration of guest triplets. If the transfer rate constant (k_{EX}) were sufficiently high, process (c) could provide a high-density population of the Ir complex triplets. However, an independent study is needed to substantiate the occurrence of such a mechanism.

B. EPH quantum efficiency

The experimentally determined EPH external quantum efficiency results from the optical output, Φ_{EPH} (eV/cm^2 s), and current density j (A/cm^2), driving an EL device, $\varphi_{\mathrm{EPH}}^{(\mathrm{ext})} = (\Phi_{\mathrm{EPH}}/\langle h\nu\rangle)/(j/e)$ (photon/electron), where $\langle h\nu\rangle$ (eV) is the photon energy averaged over the total emission spectrum, and e (C) is the elementary charge. It constitutes only a fraction of the intrinsic (internal) quantum efficiency $[\varphi_{\mathrm{EPH}}^{\mathrm{int}}]$ because a part of the light produced in the emitter is lost for the direct (in face) measurement of Φ_{EPH} due to scattering and the wave-guided modes in the material, substrate and ITO

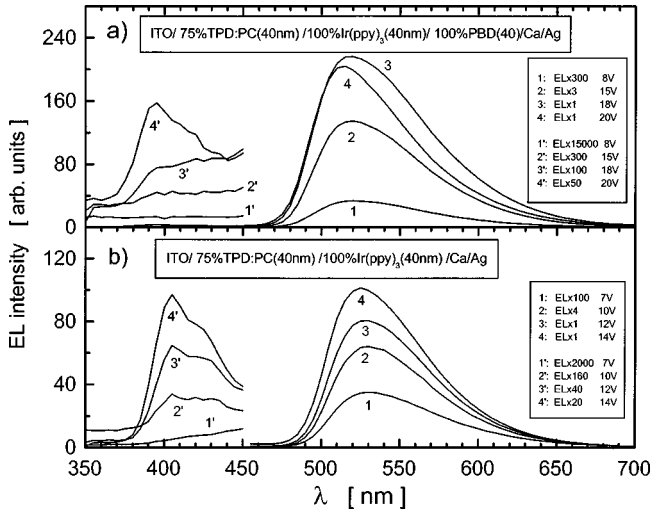

FIG. 4. The electroluminescence (EL) spectra of systems with a 100%$[\mathrm{Ir}(ppy)_3]$ component layer. (a) three-layer device: ITO/75% TPD:25% PC (40 nm)/100% $[\mathrm{Ir}(ppy)_3]$ (40 nm)/100%PBD (40 nm)/Ca/Ag, and (b) double-layer device without blocking PBD layer: ITO/75%TPD:25%PC (40 nm)/100%$[\mathrm{Ir}(ppy)_3]$(40 nm)/Ca/Ag. The residual emission from TPD:PC hole transporting layer is apparent at $\lambda \cong 400$ nm, increasing with the voltage applied to the devices.

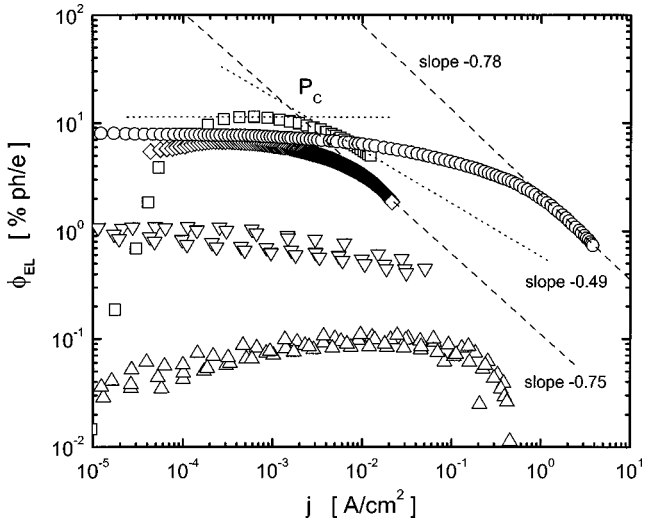

FIG. 5. The external quantum efficiency of devices using $[\mathrm{Ir}(ppy)_3]$ phosphorescent compound, as a function of the driving current. The data for 6%$[\mathrm{Ir}(ppy)_3]$: CBP (circles) are taken from Ref. 11. The squares show the data for the 6%$[\mathrm{Ir}(ppy)_3]$ in (TPD:PC) system for the first run, the diamonds are the same system for the second run, the down triangles are the data for the (TPD:PC)/$[\mathrm{Ir}(ppy)_3]$/PBD system, and the up triangles are the data for the (TPD:PC)/$[\mathrm{Ir}(ppy)_3]$ system.

electrode[32] $[\varphi_{\mathrm{EPH}}^{(\mathrm{ext})}=\xi\varphi_{\mathrm{EPH}}^{(\mathrm{int})}$, where ξ is the so-called light output coupling factor]. The external EL quantum efficiency of three different devices is shown as a function of injected current density in Fig. 5. The straight lines approximate the highest current density behavior demonstrating that except for the first run of the 6% $[\mathrm{Ir}(ppy)_3]$:(TPD:PC) device, the slopes are larger than 0.5 predicted by triplet-triplet (*T-T*) quenching according to Eq. (18) in Sec. V. The point P_c determines the critical value of the current density j_{crit} at which the *T-T* annihilation dominates the triplet exciton decay; j_{crit} is used in an evaluation of the second order *T-T* annihilation rate constant (Sec. V). The role of the $[\mathrm{Ir}(ppy)_3]$ dispersion and PBD hole blocking layer is apparent from decreasing efficiency as passing from the devices with $[\mathrm{Ir}(ppy)_3]$ dispersed in hole-transporting matrices [(TPD:PC), CBP] in the presence of the hole blocking layer of PBD, through a 100% $[\mathrm{Ir}(ppy)_3]$ emitter layer, to a system with no hole blocking layer.

The emission efficiency of the $[\mathrm{Ir}(ppy)_3]$-doped TPD:PC HTL device [Fig. 2(a)] is largely higher than those with a separated $[\mathrm{Ir}(ppy)_3]$ layer. Indeed, the peak efficiency of (11 ± 1)% photons/electron exceeds largely the best result of (0.8 ± 0.2)% photons/electron for the three-layer (TPD:PC)/100%$[\mathrm{Ir}(ppy)_3]$/100%PBD device and (0.10 ± 0.02)% photons/electron for the double-layer device (TPD:PC)/100%$[\mathrm{Ir}(ppy)_3]$. Moreover, it exceeds by about 30% the maximum $\varphi_{\mathrm{EPH}}^{(\mathrm{ext})}$ obtained from a complex fully vacuum-evaporated four-layer structure where the luminescent layer consisted of a 6% dispersion of $[\mathrm{Ir}(ppy)_3]$ in (4,4′-*N*,*N*′-dicarbazole-biphenyl)(CBP) matrix.[11]

We note that the initial increase of the quantum efficiency is directly related to the recombination (τ_{rec})-to-transit (τ_t) time ratio,[1,7] $\varphi_{\mathrm{EL}}^{(\mathrm{int})}=\alpha_2\varphi_{\mathrm{PH}}(1+\tau_{\mathrm{rec}}/\tau_t)$, which can be expressed by the actual current (j) flowing through the device as[33]

$$\frac{\tau_{\mathrm{rec}}}{\tau_t}=\frac{8e\mu_e}{9\gamma\varepsilon_o\varepsilon}\frac{j_{\mathrm{SCL}}}{j}. \tag{1}$$

Here φ_{PH} is the phosphorescence quantum efficiency, μ_e is the microscopic mobility of electrons, γ is the second-order *e-h* recombination rate constant, ε is the dielectric constant of the material, ε_o is the dielectric permittivity of vacuum, and $j_{\mathrm{SCL}}\cong(9/8)\varepsilon_o\varepsilon\mu_h F^2/d$ represents the volume-limited current which is here approximated by the unipolar space-charge-limited (SCL) current of majority carriers (holes) flowing in the device of thickness *d*. If the carrier injection at a given voltage is insufficient to establish the highest current represented by the j_{SCL} ($j<j_{\mathrm{SCL}}$), $\tau_{\mathrm{rec}}/\tau_t>(8/9)\times(\mu_e/\gamma\varepsilon_o\varepsilon)$. At increasing voltage, j approaches j_{SCL}, the τ_{rec}-to-τ_t ratio decreases leading to increasing EL quantum efficiency. If at a certain electric field $F_o=U_{\mathrm{crit}}/d$, $j=j_{\mathrm{crit}}=j_{\mathrm{SCL}}$, the $\tau_{\mathrm{rec}}/\tau_t$ ratio can become constant (whenever the μ_e/γ ratio is a field-independent or weakly varying function of electric field quantity). Such a situation with our devices occurs at current densities exceeding 10^{-4} A/cm^2 (Fig. 5) though the maximum EPH quantum efficiency can be reached at lower (the curve for $[\mathrm{Ir}(ppy)_3]$ in CBP, Fig. 5) or much higher ($>10^{-2}$ A/cm^2) (Refs. 26 and 34) current densities. The above considerations are clearly confirmed by the current-field characteristics presented in Sec. III C. Their good reproducibility in a series of consecutive measurement runs with the same device points out that an apparent drop in the EPH efficiency in the second run (seen in Fig. 5) cannot be explained by a modification of electrical properties of the system, but should be associated rather with the emission stage of the electrophosphorescence process.

The most obvious feature of the current density dependence of the $\varphi_{\mathrm{EPH}}^{(\mathrm{ext})}$, which we are mostly concerned with, is the quantum efficiency roll-off at increasing current densities. We translate selected curves from Fig. 5 into the field dependence of the EPH quantum efficiency in order to compare with the electric effect on phosphorescence (see Fig. 6). The phosphorescence output from the sandwich structure Al/100%$[\mathrm{Ir}(ppy)_3]$/Al [see Fig. 2(b)], which did not show any emission under action of an electric field only (without photoexcitation), decreases gradually as the applied field increases and drops down by as much as 30% at a field about 2×10^6 V/cm. A decrease of twice as much is observed in the $\varphi_{\mathrm{EPH}}^{(\mathrm{ext})}$ (second run) at the same electric field. This suggests at least a large part of the reduction in $\varphi_{\mathrm{EPH}}^{(\mathrm{ext})}$ to have the same origin as the electric field-induced quenching of phosphorescence, and this could be the electric-field-assisted dissociation of Coulombically correlated electron-hole pairs mentioned in Sec. I and shown in Sec. V.

C. Current-field characteristics

In Fig. 7, the current density is shown as a function of the effective electric field $[F_{\mathrm{eff}}=(U-U_{bi})/d=100\ \mathrm{nm}, F_{\mathrm{eff}}=(U/d)-(U_{bi}/d)=F-F_{bi}]$ on a double logarithmic plot for

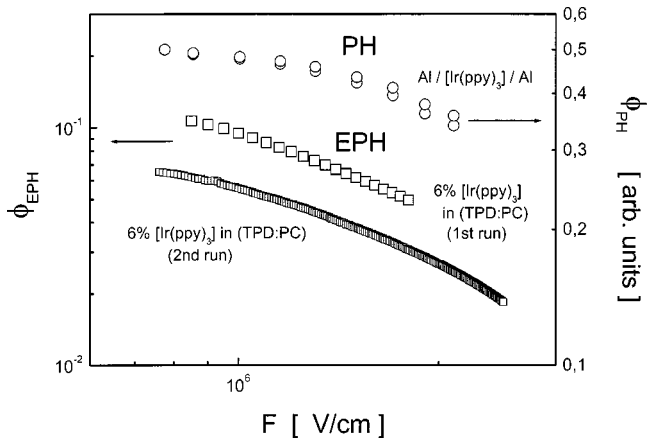

FIG. 6. Phosphorescence (PH) and electrophosphorescence (EPH) efficiency response to the dc applied electric field. The relative PH efficiency at $\lambda_{PH}=(525\pm6)$ nm was measured with an excitation wavelength of 436 nm and an exciting light intensity of $I_0\cong10^{14}$ quanta/cm^2 s.

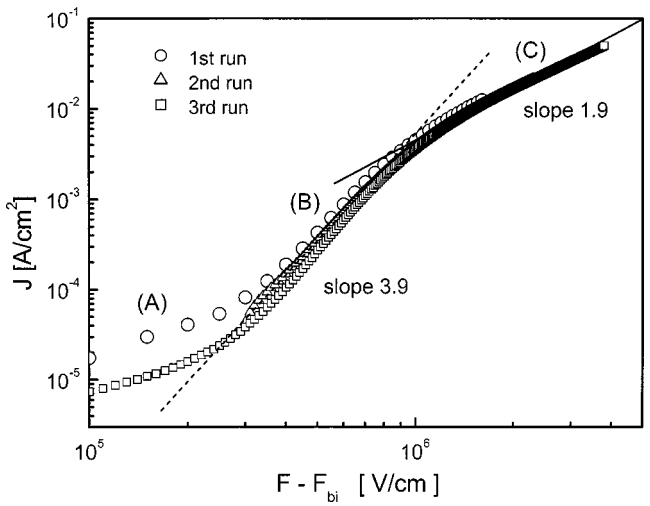

FIG. 7. A double-logarithmic plot of the field dependence of the driving current in the electrophosphorescent device 6%[Ir$(ppy)_3$]:(TPD:PC) (for the complete device structure, see the caption of Fig. 3), measured at three different consecutive runs. The constant $F_{bi}=2\times10^5$ V/cm represents the built in electric field due to the difference in the work functions of the electrodes. The lines are fits to a power law with slopes equal to 3.9 [segment (B)] and 1.9 [segment (C)]. The diverging data in segment (A) are dictated by unstable current flow conditions at low voltages.

the central electrophosphorescent device depicted in Fig. 2(a). The curves seem to reveal three different regimes, which can be attributed to[35] (A) leakage or diffusion-limited conduction, (B) volume-controlled current with an exponential distribution of traps, $j\propto F^{l+1}/d^l$, and (C) volume-controlled current with filled traps, $j\propto F^2/d$. The slope of regime (B) is $m=3.9$ and may be assigned to trapping of majority carriers (holes) traps distributed in energy (E) according to an exponential function $h(E)=(H/lkT)\times\exp(-E/lkT)$, where H is the total number of traps per unit volume, T is the absolute temperature, k is Boltzmann's constant, and l is a characteristic dimensionless parameter of the trap distribution $l=m-1=2.9$. The field $F=F_{\mathrm{TFL}}$ that corresponds to the transition between regimes (B) and (C) is usually referred to as the ''trap-filled limit'' when the last traps (shallowest but not extremely shallow) are being filled. From its value the total concentration of traps follows:[35] $H\cong(3/2)\varepsilon_o\varepsilon F_{\mathrm{TFL}}/ed\cong3\times10^{19}/\mathrm{cm}^3$. This number can be in error of about factor of two since the charge accumulated at the HTL/ETL interface can make the field to be nonuniformly distributed among these two layers. The nature of traps is not known, but the disorder occurring as a rule in molecularly doped and vacuum-deposited organic films imposes a statistical distribution of site energies within a 0.1 eV width.[36] The trapping depth representing the exponential trap distribution with $l=2.9$, $E_l=l\,\mathrm{kT}\cong0.07$ eV, corresponds well to this energy range. The energy domain probed under most experimental conditions is such that the total number of states as a function of energy is comparable for both Gaussian and exponential distribution functions; for this reason the exponential and Gaussian trap distributions lead approximately to identical current-voltage characteristics.[37] Interestingly, the currents are well reproducible from run to run, suggesting that charge injection and transport conditions do not change significantly under electrical stress. However, a limited production of exciton quenching centers, due to material deterioration processes,[38] cannot be excluded as the EPH quantum efficiency becomes reduced in successive measurement runs (see Fig. 5). There is an apparent correlation between the current regimes in Fig. 7 and the current evolution of the EPH quantum efficiency presented in Fig. 5. Within the regime (B) $\varphi_{\mathrm{EPH}}^{(\mathrm{ext})}$ remains approximately unchanged, and a well-pronounced decrease in $\varphi_{\mathrm{EPH}}^{(\mathrm{ext})}$ is observed in regime (C). As already discussed in Sec. III B, the low-current EPH quantum efficiency increases with electric field because the recombination-to-transit time ratio decreases being a consequence of the injection-controlled EL mode,[1] the SCL current regimes [(B) and (C)] should be characterized by a constant recombination-to-transit time ratio. However, the observed roll-off in the $\varphi_{\mathrm{EPH}}^{(\mathrm{ext})}$ indicates some other factors to be invoked in determining the final EPH yield. They are discussed in Secs. IV and V.

IV. QUENCHING MECHANISMS

A. Triplet-triplet annihilation

We assume that a spatially homogeneous triplet exciton density (T) is formed either during steady-state excitation by light of intensity I_0 or created via the recombination of oppositely charged carriers injected from the electrodes of a sandwich electrode organic phosphor/electrode system operating under steady-state conditions of a dc injection. The nine spin states (Ψ_i) of the ($T\ldots T$) complex preceding the final products of the *T-T* annihilation reaction, make the complex a singlet-triplet-quintet mixture due to various triplet spin configurations.[7,39] The quantum mechanical singlet $|\langle\Psi_i|S\rangle|$ and triplet $|\langle\Psi_i|T\rangle|$ spin components lead to energetically accessible singlet (S) and triplet (T) exciton final products according to the reaction scheme

$$T+T \overset{\gamma_{\mathrm{TT}}^{(S)}}{\rightleftarrows (T\ldots T) \rightleftarrows} S+S_0 \tag{2}$$

$$T+T \overset{\gamma_{\mathrm{TT}}^{(T)}}{\rightleftarrows (T\ldots T) \rightleftarrows} T+S_0 \tag{3}$$

Here $\gamma_{\mathrm{TT}}^{(S)}$ and $\gamma_{\mathrm{TT}}^{(T)}$ stand for the overall second order rate constants ($\mathrm{cm}^3\,\mathrm{s}^{-1}$) in the singlet and triplet creating annihilation processes (2) and (3). The radiative decay of singlets and triplets results in the delayed fluorescence [reaction (2)] and phosphorescence [reaction (3)]. Steady-state considerations apply to our experiments. In any thin section of the sample at a distance x from the transparent (or semitransparent) reference electrode, the concentration dependence of S and T may be described by the equations:

$$\frac{dS}{dt}=\alpha_1(1-\eta)\frac{j}{ew}+\gamma_{\mathrm{TT}}^{(S)}T^2-[k_r^{(S)}+k_{\mathrm{ISC}}+k_n^{(S)}] \times[1-\eta_{\mathrm{ex}}^{(S)}]^{-1}S=0, \tag{4}$$

$$\frac{dT}{dt}=\alpha_2(1-\eta)\frac{j}{ew}+k_{\mathrm{ISC}}S-[k_r^{(T)}+k_n^{(T)}][1-\eta_{\mathrm{ex}}^{(T)}]^{-1}T -[2\gamma_{\mathrm{TT}}^{(S)}+\gamma_{\mathrm{TT}}^{(T)}]T^2=0, \tag{5}$$

where j is the recombination current density flowing within the recombination zone of width w, e is the elementary charge, and the symbol k (s^{-1}) denotes unimolecular rate constants for radiative $[k_r^{(S)},k_r^{(T)}]$ and radiationless $[k_n^{(S)},k_n^{(T)}]$ singlet and triplet exciton transitions, respectively, and for intersystem crossing singlet-triplet conversion (k_{ISC}). It must be pointed out here that, unlike earlier kinetics assuming all the encounter charge pairs (CP) to form excitons,[16] Eqs. (4) and (5) include their spin weights and the reduction factors due to the dissociation processes of the charge pairs (see Fig. 1). The latter are accounted for by the carrier separation probability $\eta=\eta_0\Omega$ (see Fig. 1). The separation probability can be simply expressed by the dissociation unimolecular rate constant, k_d, using the definition relationship $\eta=k_d/(k_r+k_n+k_{\mathrm{ISC}}+k_d)$. We distinguish between η and η_{ex} corresponding to generally different dissociation rates of the carrier recombination produced CPs and charge transfers (CT's) created in the exciton separation process. The rate equations (4) and (5) do not contain explicitly expressed energy transfer terms and transfer rates, k_{SS}, k_{TT}, and k_b. They can be considered as forming part of non-radiative decay rates and, in the case of $\mathrm{Ir}(ppy)_3$, are accounted for by the effective lifetime of triplet excitons. The direct contribution of TPD triplets to the emission of our samples has been neglected for the following reasons. The energy of TPD triplet excitons (2.3 eV) (Ref. 30) locates their phosphorescence emission at $\cong$540 nm far beyond the fluorescence maximum ($\cong$ 400 nm).[7] The EL spectrum of a single-layer light-emitting diode based on a 100% vacuum-evaporated thin film of TPD does not show any pronounced feature around 540 nm.[7] This concurs with direct measurements of the TPD phosphorescence which appeared to be very weak at room temperature.[30] Major simplifications are achieved if we consider two limits of low (case I) and high (case II) either optical or electrical excitation levels at room temperature.

Case I: The triplet exciton concentration is too low to give rise to triplet-triplet fusion and the T^2 terms in Eqs. (4) and (5) can be dropped, so that

$$T\cong\frac{(1-\eta)j}{ew}\,\frac{\alpha_2+\alpha_1 k_{\mathrm{ISC}}/[k_r^{(S)}+k_{\mathrm{ISC}}+k_n^{(S)}]}{k_r^{(T)}+k_n^{(T)}} \tag{6}$$

if $\eta_{\mathrm{ex}}^{(S)}\cong\eta_{\mathrm{ex}}^{(T)}=\eta_{\mathrm{ex}}$.

The triplet exciton concentration increases linearly with recombination current density j. Thus, the quenching efficiency in the *T-T* annihilation process increases as j^2.

Case II: The triplet exciton lifetime is determined by the T^2 term in this regime, the monomolecular decay terms can be neglected and the solutions to Eqs. (4) and (5) are well approximated by

$$T\cong\left(\frac{(1-\eta)j}{ew}\,\frac{\alpha_2+k_{\mathrm{ISC}}\alpha_1[1-\eta_{\mathrm{ex}}^{(S)}]/[k_r^{(S)}+k_{\mathrm{ISC}}+k_n^{(S)}]}{[2\gamma_{\mathrm{TT}}^{(S)}+\gamma_{\mathrm{TT}}^{(T)}]-k_{\mathrm{ISC}}\gamma_{\mathrm{TT}}^{(S)}[1-\eta_{\mathrm{ex}}^{(S)}]/[k_r^{(S)}+k_{\mathrm{ISC}}+k_n^{(S)}]}\right)^{1/2}, \tag{7}$$

proportional to $\sqrt{j}$. A linear increase with j of the T^2 terms in Eqs. (4) and (5) is characteristic of the *T-T* quenching in this case.

B. Triplet-charge carrier interaction

Correlated triplet-doublet pairs $(T\ldots D)$ are formed prior to triplet quenching by a charge carrier,

$$T+D \overset{\gamma_{Tq}}{\rightleftarrows (T\ldots D) \rightleftarrows} S_0+D^* \tag{8}$$

where γ_{Tq} ($\mathrm{cm}^3\,\mathrm{s}^{-1}$) is the overall second order triplet-doublet interaction rate constant. The final state D^* is an excited doublet which can either relax to D or autoionize into a free carrier (electron or hole) and a ground state neutral trap. The constant γ_{Tq} is determined by the quantum

mechanical doublet spin component of the six doublet-quartet mixtures of the complex $(T \ldots D_{\pm 1/2})$.[7,39] In kinetic equations (4) and (5), quenching process (8) modifies the first-order decay constant

$$k_{\mathrm{tot}}^{(T)} = [k_r^{(T)} + k_n^{(T)} + \gamma_{Tq} n][1 - \eta_{\mathrm{ex}}^{(T)}]^{-1} \tag{9}$$

where n (cm^{-3}) is the concentration of the interacting carriers.

Assuming the process to be dominating and $\eta_{\mathrm{ex}}^{(T)} \rightarrow 0$, makes the triplet excitons to decay in a first order kinetic defined in the previous section as case I. However, its low and high excitation subcases can now be distinguished based on the contribution of the term $\gamma_{Tq} n$. (i) The triplet lifetime is essentially independent of charge density, $k_{\mathrm{tot}}^{(T)} \cong k_r^{(T)} + k_n^{(T)}$. (ii) The triplet lifetime is determined by the triplet exciton-charge carrier interaction, $k_{\mathrm{tot}}^{(T)} \cong \gamma_{Tq} n$, so that expressions for

$$T = \frac{\alpha I_0 k_{\mathrm{ISC}}}{\gamma_{Tq} n [k_r^{(S)} + k_{\mathrm{ISC}} + k_n^{(S)}]} \tag{10}$$

under photoexcitation (α-linear absorption coefficient of the exciting light), and

$$T = \frac{(1-\eta) j}{e w} \frac{\alpha_2 + \alpha_1 k_{\mathrm{ISC}} / [k_r^{(S)} + k_{\mathrm{ISC}} + k_n^{(S)}]}{\gamma_{Tq} n} \tag{11}$$

under electrical excitation, lead to a sublinear triplet concentration increase with I_0 or j, since also n is an increasing function of the excitation level.

C. Dissociation of excited states

In the electron-hole recombination process, it is commonly assumed that if the thermalized electron comes within a Coulombic capture radius $r_c = e^2/4\pi\varepsilon_0\varepsilon kT$ of the hole, then recombination is certain.[37] However, it is possible that when the hole and electron are on adjoining sites, there can be sufficient thermal energy to dissociate such a pair, the process to be characterized by a dissociation time τ_d [Fig. 1(a)]. The same may happen to a CT exciton formed at the initial stage of the charge carrier separation (η_0) from optically excited localized exciton states [Fig. 1(b)]. If such a process proceeds in an external electric field (F), the probability to escape recombination strongly increases, we deal with a field-assisted dissociation of coulombically-correlated CP pairs. The field dependence of the dissociation reflects in the field dependence of intrinsic photoconduction[37,40] or electromodulated luminescence.[23,24,40]

The functional shape of the overall dissociation probability $\eta(F)$ depends on the physical mechanism underlying the charge separation. A common one is the Poole-Frenkel effect.[41,42] In the Poole-Frenkel (PF) framework the field-dependent dissociation probability of an excited state into a pair of free carriers is given by

$$\eta_{\mathrm{PF}}(F) = \eta_0 \frac{\exp(\beta_{\mathrm{PF}} F^{1/2}/kT)}{A_{\mathrm{PF}} + \exp(\beta_{\mathrm{PF}} F^{1/2}/kT)}, \tag{12}$$

where $\beta_{\mathrm{PF}} = (e^3/\pi\varepsilon_0\varepsilon)^{1/2}$ is a characteristic Poole-Frenkel parameter determined by the dielectric constant ε of the material solely, and $(1 + A_{\mathrm{PF}})^{-1}$ represents the zero-field dissociation probability. η_0 denotes the probability of charge pair formation which as a rule is smaller than unity under optical excitation, and $\eta_0 = 1$ in the bimolecular recombination process. The charge separation is here driven by a thermal activation of a carrier over the counter charge Coulombic barrier established and decreasing with an increasing external electric field.

Another, even more employed in organics, separation mechanism is the charge carrier diffusion in the coulomb field of its parent countercharge and the applied electric field. It has been described by Onsager,[43] and its field-dependent probability expressed by[37]

$$\eta_{\mathrm{Ons}}(F) = \eta_0 \int g(r,\theta) f(r,\theta) d\tau, \tag{13}$$

where $g(r,\theta)$ is the probability per unit volume of finding the ejected electron in a volume element $d\tau$, r is the separation distance r and θ is the angle between the radius vector $\mathbf{r}$ and the applied field vector $\mathbf{F}$, and $f(r,\theta)$ is the probability that the charge pair will dissociate as a function of the separation distance and the angle θ. For an isotropic system containing a low concentration of charge pairs (no interaction between charge pairs) in thermal equilibrium with a dielectric medium of dielectric constant ε, the Onsager function $f(r,\theta)$ reads

$$f(r,\theta) = \exp[-(A+B)] \sum_{m}^{\infty} \sum_{n=0}^{\infty} \frac{A^m}{m!} \frac{B^{m+n}}{(m+n)!}. \tag{14}$$

Here $A = 2q/r$, $B = \beta r(1 + \cos\theta)$, $q = e^2/8\pi\varepsilon_0\varepsilon kT$, $\beta = eF/2kT$, and $g(r,\theta)dr\, d\theta \cong 4\pi r^2 g(r)$. The expansion coefficients in Eq. (14) are governed by the so-called ''Onsager radius'' at which the Coulombic attraction is equal to the thermal energy (kT), $r_c = e^2/4\pi\varepsilon_0\varepsilon kT$, and a distribution function for the initial separation of the CP states. Assuming the initial separation distance to be a discrete value $r_0 = r_{e\text{-}h}$ (or r_{CT}), that is a delta function for $g(r) = \delta(r - r_0)/4\pi r_0^2$, one arrives at a definition equation for the zero-field separation probability $\eta(F=0) = \eta_0 \exp(-r_c/r_0)$. An analysis of $\eta(F)$ shows its Poole-Frenkel plots to be much steeper, and reaching the saturation point at a lower field than those based on the Onsager theory.[44] In the latter case, the steepness and the saturation point are determined by η_0 and r_0. For larger values of r_0 a less steep $\eta(F)$ curve reaches saturation at lower field strength.

V. DISCUSSION

The rapid decrease seen in the EPH quantum efficiency as the current density increases (Fig. 5) can be ascribed to either

of quenching mechanisms described in Sec. IV. The quantum efficiency as defined in Sec. III B is directly related to the concentration (T) of triplet excitons:

$$\varphi_{\mathrm{EPH}}^{(\mathrm{ext})}=\xi\varphi_{\mathrm{PH}}\frac{eTw_e}{\tau_{\mathrm{PH}}j}. \tag{15}$$

This is a definition relationship assuming a homogeneous population of triplets (T) throughout the emission zone, w_e. Let us recall that, in general, the emission zone does not coincide with the recombination zone (w). If the latter is very narrow, as in the present case, the emission zone is larger than w, being limited on the large values side by the thickness of the emitting layer $d/2=50$ nm. On the other hand, the external EPH efficiency can be expressed by the effective triplet exciton lifetime (τ_{tot}) as

$$\varphi_{\mathrm{EPH}}^{(\mathrm{ext})}=\xi\alpha_2(1-\eta)\varphi_{\mathrm{PH}}\frac{\tau_{\mathrm{tot}}}{\tau_{\mathrm{PH}}} \tag{16}$$

where $\varphi_{\mathrm{PH}}=k_r^{(T)}/[k_r^{(T)}+k_n^{(T)}]$, and

$$\tau_{\mathrm{tot}}^{-1}=[\tau_{\mathrm{PH}}^{-1}+\gamma_{Tq}n][1-\eta_{\mathrm{ex}}^{T}]^{-1}+[2\gamma_{\mathrm{TT}}^{(S)}+\gamma_{\mathrm{TT}}^{(T)}]T \tag{17}$$

is the effective (total) triplet exciton rate constant including all monomolecular and bimolecular quenching processes such as triplet-charge carrier or triplet-triplet annihilation (see Sec. IV), and τ_{PH} represents the intrinsic triplet exciton lifetime in the absence of quenching. Assuming that the dissociation efficiency is independent of current density, thus the electric field applied to the system [$\eta(F)=$const], the current dependence of the EPH quantum efficiency [$\varphi_{\mathrm{EPH}}^{(\mathrm{ext})}$] should be projection of that for the effective lifetime of triplets [$\tau_{\mathrm{tot}}(j)$]. The experimental data for the EPH lifetime and quantum efficiency show a pronounced discrepancy (Fig. 8). The quantum efficiency drops down by about 90% at $j\cong 150$ mA/cm^2, whereas the effective lifetime decreases by less than 40% only at the same current density. A decreasing tendency in the phosphorescence lifetime as the photoexciting energy pulse increases suggests both EPH and PH lifetimes to be underlain by triplet-triplet annihilation process (Sec. IV A).

Another test of the significance of triplet-triplet and triplet-charge carrier annihilation is to follow the current density dependence of the concentration (T) of triplet excitons, and thus, directly, the EPH quantum efficiency [Eq. (15)] as a function of the current density. The linear current increase of T in the absence of the T-T quenching (case I, Sec. IV A), leads to $\varphi_{\mathrm{EPH}}^{(\mathrm{ext})}=$const as, indeed, can be observed at low current densities below a field F_0 at which $j=j_{\mathrm{crit}}$, and where a pronounced decrease in the EPH efficiency becomes detectable (Fig. 5). On the other extreme (case II, Sec. IV A), T is proportional to $j^{1/2}$ [Eq. (7)]; thus, according to Eq. (15), $\varphi_{\mathrm{EPH}}^{(\mathrm{ext})}\propto j^{-1/2}$. As a consequence, the efficiency decrease at highest current densities would be expected to be a straight line logarithmic plot {log[$\varphi_{\mathrm{EPH}}^{(\mathrm{ext})}$] vs log j} with the slope $-\frac{1}{2}$. For all the experimental curves of Fig. 5 it is not the case, the greater slopes suggesting an additional quenching mechanism operating in the device. An exception is observed for the first lower-current range run, where the slope approaches $-\frac{1}{2}$. From its intersection (P_c) with the horizontal line representing $\varphi_{\mathrm{EPH}}^{(\mathrm{ext})}=$const$=11\%$ photons/electron, one can evaluate the T-T annihilation rate constant γ_{TT}. At the intersection point $\varphi_{\mathrm{EPH}}^{(\mathrm{ext})}(j=j_{\mathrm{crit}})=0.11$. The $\varphi_{\mathrm{EPH}}^{(\mathrm{ext})}$ (case II, Sec. IV A) can be approximated by

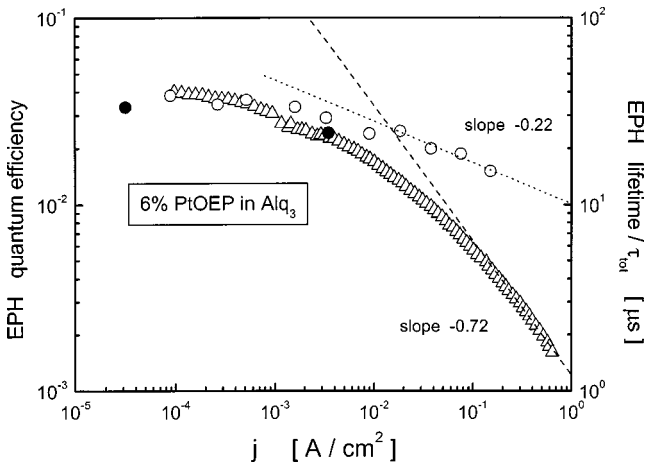

FIG. 8. Lifetime (open circles) and EL quantum efficiency (triangles) of the phosphorescent dye 2,3,7,8,12,13,17,18-octaethyl-21H, 23H-porphine platinum (II) (PtOEP) embedded in an Alq_3 matrix as a function of the current density. Two filled circles are the lifetimes of the phosphorescence taken at increasing photoexcitation pulse (left: 160 nJ/cm^2; right: 16 μJ/cm^2). A strong divergence at high current densities is apparent. The data is adapted from Ref. 9.

$$\varphi_{\mathrm{EPH}}^{(\mathrm{ext})}(II)\cong\frac{\xi\varphi_{\mathrm{PH}}}{2\tau_{\mathrm{PH}}}\left(\frac{ew}{j_{\mathrm{crit}}\gamma_{\mathrm{TT}}}\right)^{1/2} \tag{18}$$

if $\eta\ll 1$, $\alpha_2=\frac{3}{4}$, $\gamma_{\mathrm{TT}}^{(S)}\cong\gamma_{\mathrm{TT}}$ is assumed and contribution of the intersystem crossing transitions to the triplet exciton concentration is neglected [cf. Eq. (7)]. The triplet-triplet annihilation rate constant could be estimated from Eq. (18) on the basis of the experimental value of j_{crit} if the recombination zone width were known. The recombination zone, though difficult to evaluate exactly, can be assumed to be very narrow because of the confinement of charge carriers at the [TPD:Ir(ppy)$_3$:PC]/PBD interface, imposed by the relatively high-energy barriers for both holes and electrons [see Fig. 2(a)]. This is confirmed by the volume controlled current flow in the device (Fig. 7). Therefore, a lower limit for w can be compared with the dimension of the two nearest-neighbor molecules ($\cong$ 2 nm). The upper limit results from the thickness of the emitter layer ($\cong d/2\cong 50$ nm). Thus we find 1×10^{-14} cm^3/s$\leqslant\gamma_{\mathrm{TT}}\leqslant 2.5\times10^{-13}$ cm^3/s, using $\tau_{\mathrm{PH}}=15\,\mu$s (Ref. 30), $\varphi_{\mathrm{PH}}=40\%$ (Ref. 26), $j_{\mathrm{crit}}=2\times10^{-3}$ A/cm^2, and $\varphi_{\mathrm{EPH}}^{(\mathrm{ext})}(j=j_{\mathrm{crit}})=0.11$ from Fig. 5. A typical value of the light output coupling factor $\xi\cong 0.2$ has been used in this evaluation.[20] These values of γ_{TT} agree reasonably with that for another organic phosphorescent system,

PtOEP:CBP, $\gamma_{TT} \cong 3\times10^{-14}$ cm^3/s obtained from the fitting of the experimental data of $\varphi_{EPH}^{(ext)}(j)$ to the triplet-triplet quenching mechanism.[16] We recall that the long phosphorescence lifetime of the guest molecules of [Ir$(ppy)_3$] in the host TPD has been thought to be determined by the energy transfer rate from the long-living triplet excitons of TPD.[30] Therefore, the above calculated constant γ_{TT} may be ascribed to the annihilation reaction between TPD triplets rather than excited triplets of [Ir$(ppy)_3$] which reveal a much shorter intrinsic lifetime, $\tau_{PH}<1$ μs (Refs. 11 and 30). A possibility of the direct guest annihilation triplets or host-guest triplet hetero annihilation process would lead to the γ_{TT} of two orders of magnitude higher, $\gamma_{TT}\cong10^{-11}$ cm^3/s. Finally, it is necessary to note that previous attempts to fit the $\varphi_{EPH}^{(ext)}(j)$ plots to the triplet-triplet quenching mechanism failed for the [Ir$(ppy)_3$]:CBP electrophosphorescent system and revealed remarkable deflections at the highest current densities for other electrophosphorescent systems.[16]

Let us now consider the triplet-charge carrier annihilation to be a dominating quenching process (Sec. IV B). In order to test this mechanism the current dependence of the charge concentration (n) must be known [see Eq. (11)]. Using the high-field current-field characteristic region [$j=(9/8)\varepsilon_0\varepsilon\mu_h F^2/d$; thus $n\cong(3/2)\varepsilon_0\varepsilon F/ed$, where d is the device thickness][35] (Fig. 7), with the assumptions made above for the approximation of T in the T-T annihilation process, and definition (15) yields

$$\varphi_{EPH}^{(ext)}=\frac{2}{3}\frac{\alpha_2\xi(1-\eta)\varphi_{PH}ed}{\varepsilon_0\varepsilon\gamma_{Tq}\tau_{PH}F}\frac{w_e}{w}. \tag{19}$$

A plot of $\varphi_{EPH}^{(ext)}$ versus F^{-1} is thus expected to give a straight line with the slope dependent on three material ($\varepsilon,\gamma_{Tq},\tau_{PH}$) and one sample ($d$) parameter of the system. Such straight line plots poorly approximate experimental data (Fig. 9) and their slopes lead to $\gamma_{Tq}\cong5\times10^{-12}$ cm^3/s for the first run and $\gamma_{Tq}\cong7.5\times10^{-12}$ cm^3/s for the second run at $\varepsilon=3$, $\tau_{PH}=15$ μs (Ref. 30), and $d=100$ nm. These numbers have been obtained using $w=w_{min}=2$ nm and $w_e\leqslant50$ nm.

If one assumes that both γ_{TT} and γ_{Tq} are governed by the triplet exciton motion, then the diffusion coefficient of triplet excitons (D_T) can be calculated from their values, $\gamma_{Tq}\cong\gamma_{TT}\cong8\pi RD_T$ (Ref. 37): 4×10^{-9} cm^2/s$\leqslant D_T\leqslant3\times10^{-6}$ cm^2/s. The hopping exciton distance has arbitrarily been taken as $R=1$ nm in the calculation. These values of the triplet exciton diffusion coefficient are much lower as compared with those for singlet excitons (D_S) which in another metallic complex Alq_3 fall in the range 1.2×10^{-5} cm^2/s$\leqslant D_S\leqslant3\times10^{-4}$ cm^2/s (Refs. 31 and 45–47). It is not surprising, the diffusion coefficients of triplets are expected to be lower than of singlets since both energy donor and acceptor transitions are disallowed.[37]

The domination of the PH quenching by the triplet-triplet annihilation or by electrons injected from the Al cathode (see Fig. 6) is highly improbable due to the irradiation conditions and charge injection properties of the Al/Ir$(ppy)_3$ contact. The used exciting light intensity $I_0\cong10^{14}$ quanta/cm^2/s ($\lambda_{exc}=436$ nm) produces the triplet exciton concentration of about $T=I_0\alpha\tau\cong5\times10^{12}$/cm^3, with an absorption coefficient $\alpha\cong5\times10^4$ cm^{-1} and $\tau\cong1$ μs. In order that the triplet-triplet annihilation could dominate the triplet exciton decay, its second order rate constant should be as high as $\gamma_{TT}\cong(\tau T)^{-1}\cong2\times10^{-7}$ cm^3/s. This is a value exceeding γ_{TT} for the phosphorescent molecules of PtOEP [2,3,7,8,12,13,17,18-octaethyl-21H, 23H-porphine platinum (II)] by nearly seven orders of magnitude,[16] and by about four orders of magnitude typical values of the T-T annihilation rate constants in single organic crystals.[37] There are no particular reasons for Ir$(ppy)_3$ to reveal such a high mobility of excitons and, therefore triplet-triplet annihilation as a process determining its phosphorescence quenching is highly unlikely. The weakly injection Al cathode (the injection barrier for electrons, as determined from the Al work function $W_{Al}\cong4.3$ eV and the Ir$(ppy)_3$ LUMO level, $\Delta E\cong1.3$ eV) supplies the sample with a measured injection current less than 0.01 μA/cm^2, and irradiated with the light exciting phosphorescence shows a photocurrent $j_{ph}\cong1$ μA/cm^2. To obtain a quenching efficiency on the level of 30% a current above 50 mA/cm^2 is needed as comes from electrophosphorescent experiments[16] (also see Figs. 5 and 10). This value is six orders of magnitude larger than the dark injection current in the Al/Ir$(ppy)_3$/Al system and four orders of magnitude higher than than the photocurrent. Therefore, the triplet-charge carrier interaction can be safely ruled out as the process determining the quenching of phosphorescence in our system described in Fig. 1(b). If for some (unknown) reasons the mobility of electrons in a 100% Ir$(ppy)_3$ were very low (say $\cong10^{-12}$ cm^2/V s) and, thus, the charge concentration in the sample was much higher than in electrophosphorescent diodes, a 30% quenching effect ($\delta=0.3$) would require the charge concentration $n=\delta/\gamma_{Tq}\tau\cong3\times10^{18}$/cm^3 with $\gamma_{Tq}\cong10^{-13}$ cm^3/s which is about two orders of magnitude higher than the maximum capacitor charge $n_c\cong\varepsilon_0\varepsilon F/ed\cong8\times10^{16}$/cm^3. This, again, makes the hypothesis of charge quenching origin of the phosphorescence quenching inapplicable.

It is often suggested that the heat dissipated in the EL cells under high current conditions can be responsible for a reduction in the EL quantum efficiency. In our experiments with a 6% content of Ir$(ppy)_3$ in the HTL, the maximum current density did not exceed 50 mA/cm^2 at about $U=40$ V (see Figs. 5 and 7). Thus, at most 2 W/cm^2 is dissipated in our EPH cells. The blackbody radiation, the heat conduction of metal electrodes and leads as well as convection heat outflow due to the ambient gas can balance only in part the electrical power input. Consequently, a temperature increase of the sample would be expected. Such a temperature increase has been indeed observed in molecularly-doped-polymer-based light emitting diodes (LED's) (Ref. 21, part I) and in common organic LED's based on the TPD/Alq$_3$ junction.[48] For the first type of LED's, the maximum temperature at a very high current of 470 mA/cm^2 was found to increase only to about 40 °C as measured with a special IR pyrometer. In the second case, it did not exceed 40 °C for the currents below 50 mA/cm^2. Only insignificant change in the PL efficiency has been observed with such a

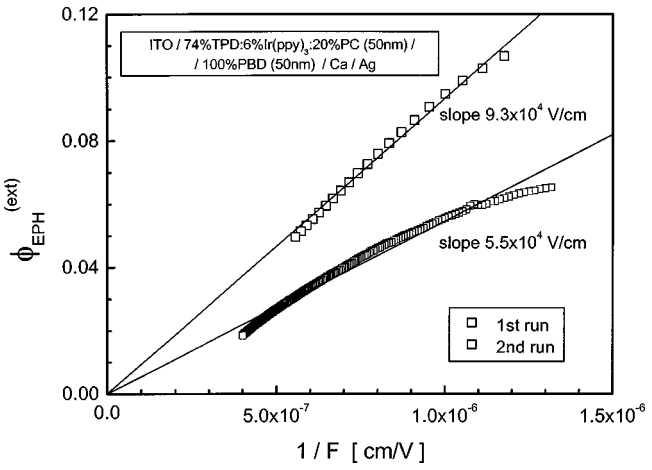

FIG. 9. Quantum electrophosphorescence efficiency data from Fig. 6 represented by a $\varphi_{\mathrm{EPH}}^{\mathrm{ext}}-F^{-1}$ plot in order to fit with the triplet–charge-carrier interaction limit for triplet exciton decay according to Eq. (19) (solid lines).

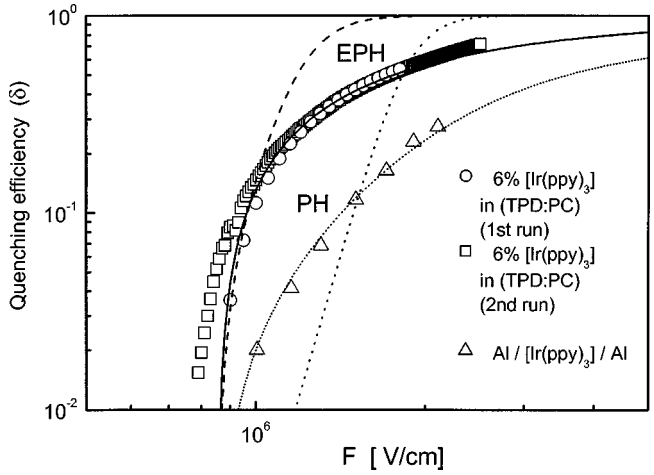

FIG. 10. Quenching efficiency [defined by Eq. (20)] as a function of the dc electric field applied to the electrophosphorescent (EPH) and phosphorescent (PH) system from Figs. 2(a) and 2(b) (circles and squares, and triangles, respectively). The curves are fits to the Poole-Frenkel and Onsager models for charge pair dissociation in external electric fields. The Poole-Frenkel plots obtained for two different values of $A_{\mathrm{PF}}=10^8$ (dashed line) and 10^{10} (dotted steep line). The Onsager formalism required different parameters for EPH (solid line): $\eta_0=1.0$ and $r_0/r_c=0.18$. For PH (dotted line) if required $\eta_0=0.9$, and $r_0/r_c=0.095$. In both cases $\varepsilon=3$ and $T=298$ K have been assumed.

15% increase in the absolute emitter temperature (see e.g., Ref. 49), the effect possibly contributing to a much larger reduction of the EL efficiency. The fluorescence efficiency decreases because the increasing population of the vibrational levels of the singlet states increases the number of possible modes or radiationless transitions. This decrease is supposed to be less than that for phosphorescence or even to disappear as for the same reason the intersystem crossing between the first excited singlet and triplet increases, producing more phosphorescent states. Moreover, the temperature dependence of the nonradiative decay rate constant for several transition metal complexes has been found to be very weak.[50] As far as electrical properties of the LED are concerned, increasing temperature increases only the carrier hopping mobilities within the SCL current regime. This can cause a decrease in the Langevin-type recombination probability,[1,7] $P_R=[1+\mu_h(T)/\mu_e(T)]/[2+\mu_h(T)/\mu_e(T)]$, if the hole ($\mu_h$)-to-electron ($\mu_e$) mobility ratio is comparable to unity and decreases with temperature. Due to the undetectable mobility of electrons in TPD-doped PC and their deep trapping on Ir(ppy)$_3$ molecules one would expect the hole mobility to be much larger than that for electrons in our LED emitter. Consequently, $P_R(T)\cong 1=\mathrm{const}$ throughout a relatively large temperature range. As a result, the overall EL yield will not necessarily show up as a temperature decreasing quantity. But even in the case of a negative imbalance factor, a possible drop in the EL efficiency should not be of crucial importance due to a narrow range of the temperature evolution at not too high driving currents.

Therefore, it may be concluded that a possible heat-induced reduction in the φ_{EL}, and triplet-triplet and triplet-charge carrier annihilation processes are insufficient to explain the experimentally observed decrease of the EL quantum efficiency of electrophosphorescent systems at high current densities and PH efficiency at high electric fields using weakly injecting electrodes Al. The field-increasing dissociation efficiency (η) of charge pairs (Sec. IV C) appears to be a straightforward candidate reducing significantly the EPH quantum efficiency as the applied voltage increases [see Eq. (16)]. In the high-field limit it can be considered as a dominating quenching factor. This means that the $\tau_{\mathrm{tot}}(F)/\tau_{\mathrm{tot}}(F_0)$ ratio is a weakly varying function of electric field, close to unity. The quenching efficiency is then simply expressed by

$$\delta=\frac{\varphi_{\mathrm{EPH}}^{(\mathrm{ext})}(F_0)-\varphi_{\mathrm{EPH}}^{(\mathrm{ext})}(F)}{\varphi_{\mathrm{EPH}}^{(\mathrm{ext})}(F_0)}\cong\frac{\eta(F)-\eta(F_0)}{1-\eta(F_0)}. \qquad (20)$$

δ varies between 0 and 1 for $\eta(F)=\eta(F_0)$ for no quenching and $\eta(F)=1$ for the total quenching, respectively. Based on the data of Fig. 6, the quenching efficiency of two devices depicted in Fig. 2 can be calculated (Fig. 10). We fit its field dependence to Eq. (20) using, for the $\eta(F)$, expressions (12) and (13) representing two different mechanisms of the field-assisted CP dissociation process (Sec. III C). Clearly, the Poole-Frenkel model must be ruled out due to a very steep field increase and a low value of the saturation field regardless of the value of the fitting parameter (A_{PF}), corresponding to two different values of the zero-field dissociation efficiency $(1+A_{\mathrm{PF}})^{-1}=10^{-8}$ and 10^{-10} that differ by as much as two orders of magnitude [the fitting procedure has been performed with $\beta_{\mathrm{PF}}=7\times10^{-23}\ C(\mathrm{V\,cm})^{1/2}$ at $\varepsilon=3$, and $kT=0.025$ eV]. They correspond to two different initial inter-carrier distance $r_{e-h}\cong 1$ and $\cong 0.8$ nm, respectively, assuming $\eta_0=1$ and $r_c=e^2/4\pi\varepsilon_0\varepsilon kT\cong 19$ nm as obtained at $\varepsilon=3$, and $kT=0.025$ eV. In contrast, the fit with $\eta(F)=\eta_{\mathrm{Ons}}(F)$ [Eq. (13)] resulting from the Onsager theory is accurate for the first run and reasonably good for the second run of the $\varphi_{\mathrm{EPH}}^{(\mathrm{ext})}(F)$ curves (Fig. 6). The curvature of the

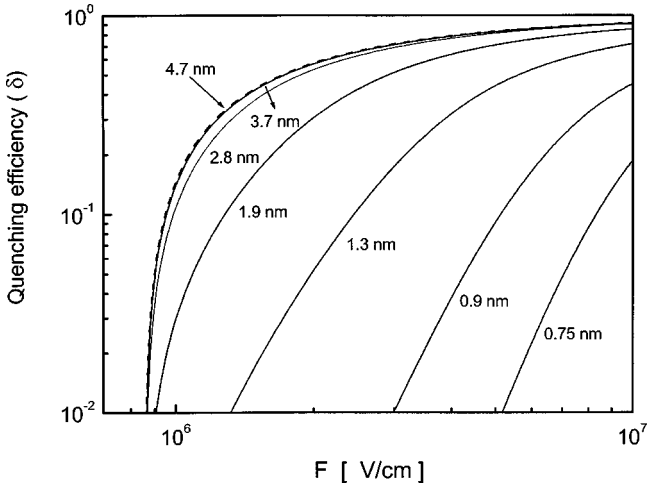

FIG. 11. Onsager plots of the quenching efficiency at $\eta_0=1$, $r_c=19$ nm, and varying r_0 (by curve numbers in nanometers). $F_0=8.55\times10^5$ V/cm is assumed to compare the curves with the experimental data of Fig. 10. The plot curvature becomes insensitive to r_0 above about 3.5 nm.

$\delta(F)$ plot is a function of two parameters r_0 and F_0. The fit for the two consecutive measurement runs for the electrophosphorescent device was made for same $r_0=3.5$ nm and $F_0=8.55\times10^5$ V/cm (based on the experimental data of Fig. 6). It is necessary to note that the value of $r_0=3.5$ nm stands for a lower limit of the electron-hole distance in the coulombically-correlated charge pair states [Fig. 1(a)]. This is because the curvature of the $\delta(F)$ function in the Onsager formalism becomes insensitive to r_0 above 3.5 nm (see Fig. 11). Thus, the average initial *e-h* distance of the CP's formed in the bi-molecular recombination can be larger, that is $r_{e\text{-}h}\geqslant3.5$ nm. At such distances the attraction Coulomb energy between the charges forming CP's becomes comparable with the energy gained from the applied external electric field. The increasing r_0 (or equivalently temperature) does not practically change the dissociation efficiency at a given field strength. The excellent fit of the phosphorescence quenching [cf. Fig. 2(b)] data with the field-assisted CT dissociation as described in the Onsager theory, is obtained with $r_0=r_{\mathrm{CT}}=(1.8\pm0.1)$ nm and $F_0=8.55\times10^5$ V/cm. The roughly twofold decrease in r_0 accompanying the observed diminution in the quenching efficiency when passing from electrophosphorescent to phosphorescent systems, illustrates the different origin of the CP states. Whereas coulombically-correlated *e-h* pairs in the EPH device originate in the mutual approaching process of statistically independent carriers injected from the electrodes [Fig. 1(a)], CT states produced under photoexcitation [Fig. 1(b)] originate from an electron-hole separation process of the initially excited molecular excitons. From the above values of r_0, we find the zero-field dissociation efficiency to differ by about two orders of magnitude for the bimolecularly formed CP's, $\eta_{e\text{-}h}(F=0)\cong4\times10^{-3}$, and for CT states, $\eta_{\mathrm{CT}}(F=0)\cong3\times10^{-5}$, as calculated with $r_c=19$ nm, and $\eta_0=1$ and $\eta_0=0.9$, respectively. This means that of one million CP's 4000 dissociate when formed by the carrier approach, and only 30 when formed by the charge separation process from molecular excitons. It must be noted that a possibility of the reduction in the PH efficiency by a dissociation of the initially excited higher electronic states produced by LC ligand-centered transitions can be here excluded since the exciting light (see Fig. 6) falls in the metal-to-ligand charge transfer optical transitions,[51] where the quenching efficiency does not vary with excitation wavelength (the data will be published in a forthcoming publication).

These results suggest that in addition to molecular properties of electrophosphorescent molecules, the intermolecular material structure must be of great care in the optimized design of electrophosphorescent devices. The shorter is the intermolecular distance, the localized recombining carrier can approach closer each other forming a closely spaced pair more difficult to dissociate due to the increased Coulombic attraction. As a consequence, the system becomes less sensitive to electric field-induced quenching. However, if specific intermolecular interactions or molecular organization impose near resonance between Frenkel and CT states, the charge separation can be a weakly field-dependent process governed by the Onsager mechanism with a relatively small initial separation distance.

VI. CONCLUSION

We have elucidated the quantum efficiency roll off in organic electrophosphorescent systems. By fitting the measured current and electric field dependent quantum efficiency data to theoretical predictions based on different quenching mechanisms, including triplet-triplet (*T-T*) and triplet-charge carrier (*T-q*) annihilation, the field-assisted dissociation of the intermediate states—Coulombically correlated oppositely charged elementary carriers is identified as the principal cause of this roll off at high electric fields. Although *T-T* and *T-q* annihilation processes contribute to the effect (especially at lower fields), as discussed already in the literature,[16] they are far insufficient to explain the experimental observations. Evidence is provided that of two well-established Poole-Frenkel and Onsager dissociation mechanisms, only the Onsager approach leads to good agreement with experiment. The fitting procedure enables to evaluate the average initial inter-carrier distance ($r_{e\text{-}h}$) of the charge pairs (CP's) formed in the bi-molecular electron-hole (*e-h*) recombination process. For the electrophosphorescent complex [$\mathrm{Ir}(ppy)_3$], $r_{e\text{-}h}\geqslant3.5$ nm.

This work has also provided evidence that the CP dissociation obeying the Onsager theory is the basic mechanism that underlies the electric-field-induced quenching of phosphorescence; the CP's identified here as charge-transfer (CT) states with a much smaller separation distance, $r_{\mathrm{CT}}=(1.8\pm0.1)$ nm for the [$\mathrm{Ir}(ppy)_3$] complex. The relation between $r_{e\text{-}h}$ and r_{CT} exemplified on the phosphorescent [$\mathrm{Ir}(ppy)_3$], is expected to hold for other phosphorescent compounds since it is caused by the fundamental difference in CP formation processes. In contrast to electrophosphorescence, where CP's are a result of the gradual approach of electrons and holes injected far away at opposite electrodes, the CP's in phosphorescence are CT states, being charge separation

products of localized excitons created under photoexcitation. Closely spaced molecular systems are thus expected to minimize the electric-field-induced effect on their phosphorescence and electrophosphorescence, except for those revealing strong CT-Frenkel exciton mixing.

ACKNOWLEDGMENTS

This work was supported in part by funds from the National Research Council (CNR) of Italy programs MIUR and PF-MSTA II Project DEMO.

[1] J. Kalinowski, J. Phys. D **32**, R179 (1999).
[2] M. A. Baldo, D. F. O'Brien, M. E. Thompson, and S. R. Forrest, Phys. Rev. B **60**, 14 422 (1999-II).
[3] Y. Cao, I. D. Parker, G. Yu, C. Zhang, and A. Heeger, Nature (London) **397**, 41 (1999).
[4] V. Griseri, L. A. Dissado, J. C. Fothergill, C. Laurent, and G. Teyssèdre, J. Phys. D **34**, 2534 (2001).
[5] M. Wohlgenannt, K. Tandon, S. Mazumdar, S. Ramasesha, and Z. V. Vardeny, Nature (London) **409**, 494 (2001).
[6] Z. Shuai, D. Beljonne, R. J. Silbey, and J. L. Bredas, Phys. Rev. Lett. **84**, 131 (2000).
[7] J. Kalinowski, in *Organic Electroluminescent Materials and Devices*, edited by S. Miyata and H. S. Nalwa (Gordon & Breach, Amsterdam, 1997), Chap. 1.
[8] J. Kalinowski, in *Polymers and Other Advanced Materials: Emerging Technologies and Business Opportunities*, edited by P. N. Prasad, E. Mark, and J. F. Fung (Plenum, New York, 1995), p. 361.
[9] M. A. Baldo, D. F. O'Brien, Y. You, A. Shoustikov, S. Silbey, M. E. Thompson, and S. R. Forrest, Nature (London) **395**, 151 (1998).
[10] D. F. O'Brien, M. A. Baldo, M. E. Thompson, and S. R. Forrest, Appl. Phys. Lett. **74**, 442 (1999).
[11] M. A. Baldo, S. Lamansky, P. E. Burrows, M. E. Thompson, and S. R. Forrest, Appl. Phys. Lett. **75**, 4 (1999).
[12] V. Cleave, G. Yahioglu, P. Le Barny, R. Friend, and N. Tessler, Adv. Mater. **11**, 285 (1999).
[13] M. A. Baldo, M. E. Thompson, and S. R. Forrest, Nature (London) **403**, 750 (2000).
[14] M. Ikai, S. Tokito, Y. Sakamoto, T. Suzuki, and Y. Toga, Appl. Phys. Lett. **79**, 156 (2001).
[15] C. Adachi, M. A. Baldo, M. E. Thompson, and S. R. Forrest, J. Appl. Phys. **90**, 5048 (2001).
[16] M. A. Baldo, C. Adachi, and S. R. Forrest, Phys. Rev. B **62**, 10 967 (2000).
[17] G. E. Jabbour, B. Kippelen, N. R. Armstrong, and N. Peyghambarian, Appl. Phys. Lett. **73**, 1185 (1998).
[18] E. Bellmann, S. E. Shaheen, S. Thaynmanavan, S. Barlow, R. H. Grubbs, S. R. Marder, B. Kippelen, and N. Peyghambarian, Chem. Mater. **10**, 1668 (1998).
[19] J. Kalinowski, M. Cocchi, V. Fattori, P. Di Marco, and G. Giro, Jpn. J. Appl. Phys., Part 1 **40**, L282 (2001).
[20] J. Kalinowski, L. C. Picciolo, H. Murata, and Z. H. Kafafi, J. Appl. Phys. **89**, 1866 (2001).
[21] J. Kalinowski, M. Cocchi, G. Giro, V. Fattori, and P. Di Marco, J. Phys. D **34**, 2274 (2001) (part I); **34**, 2282 (2001) (part II).
[22] J. Kalinowski, H. Murata, L. C. Picciolo, and Z. H. Kafafi, J. Phys. D **34**, 3130 (2001).
[23] W. Stampor, J. Kalinowski, P. Di Marco, and V. Fattori, Appl. Phys. Lett. **70**, 1935 (1997).
[24] W. Stampor, Chem. Phys. **256**, 351 (2000).
[25] K. A. King, P. J. Spellane, and R. J. Watts, J. Am. Chem. Soc. **107**, 1431 (1985).
[26] P. I. Djurovich, S. A. Lamansky, M. R. Nugent, D. L. Murphy, R. C. Kwong, and M. E. Thompson, Polym. Prepr. (Am. Chem. Soc. Div. Polym. Chem.) **41**, 770 (2000).
[27] T. Wakimoto, in *Organic Electroluminescent Materials and Devices* (Ref. 7), p. 302.
[28] Z. L. Zhang, X. Y. Jiang, S. H. Xu, and T. Nagamoto, in *Organic Electroluminescent Materials and Devices*, edited by S. Miyata and H. S. Nalwa (Gordon & Breach, Amsterdam, 1997), p. 228.
[29] G. Giro, M. Cocchi, J. Kalinowski, P. Di Marco, and V. Fattori, Chem. Phys. Lett. **318**, 137 (2000).
[30] M. A. Baldo and S. R. Forrest, Phys. Rev. B **62**, 10 958 (2000).
[31] C. W. Tang, S. A. Van Slyke, and C. H. Chen, J. Appl. Phys. **65**, 3610 (1989).
[32] V. Bulović, V. B. Khalfin, G. Gu, P. E. Burrows, D. Z. Garbuzov, and S. R. Forrest, Phys. Rev. B **58**, 3730 (1998-I).
[33] J. Kalinowski, in *Multiphoton and Light Driven Multielectron Process in Organics: New Phenomena, Materials and Applications*, edited by F. Kajzar and M. V. Agranovich (Kluwer, Dordrecht, 2000), p. 325.
[34] S. Lamansky, R. C. Kwong, M. Nugent, P. I. Djurovich, and M. E. Thompson, Org. Electron. **2**, 53 (2001).
[35] W. Helfrich, in *Physics and Chemistry of the Organic Solid State*, edited by D. Fox, M. M. Labes, and A. Weissberger (Interscience, New York, 1967), p. 1.
[36] P. M. Borsenberger, E. H. Magin, M. Van der Auweraer, and F. C. De Schryver, Phys. Status Solidi A **140**, 9 (1993).
[37] M. Pope and C. E. Swenberg, *Electronic Processes in Organic Crystals* (Clarendon, Oxford, 1982).
[38] T. P. Nguyen, P. Molinie, and P. Destruel, in *Handbook of Advanced Electronic and Photonic Materials and Devices*, edited by H. S. Nalwa (Academic, New York, 2001), Vol. 10, Chap. 1.
[39] N. E. Geacintov and C. E. Swenberg, in *Organic Molecular Photophysics*, edited by J. B. Birks (Wiley, New York, 1975), Vol. 2, Chap. 8.
[40] J. Szmytkowski, W. Stampor, J. Kalinowski, and Z. H. Kafafi, Appl. Phys. Lett. **80**, 1465 (2002).
[41] H. H. Poole, Philos. Mag. **32**, 112 (1916).
[42] J. Frenkel, Phys. Rev. **54**, 647 (1938).
[43] L. Onsager, Phys. Rev. **54**, 554 (1938).
[44] J. Kalinowski, W. Stampor, and J. Szmytkowski, Pol. J. Chem. **76**, 249 (2002).
[45] I. Sokolik, R. Priestley, A. D. Walser, R. Dorsinville, and C. W. Tang, Appl. Phys. Lett. **69**, 4168 (1996).

[46] A. D. Walser, R. Priestley, and R. Dorsinville, Synth. Met. **102**, 1552 (1999).
[47] J. Kalinowski, V. Fattori, and P. Di Marco, Chem. Phys. **266**, 85 (2001).
[48] X. Zou, J. He, L. S. Liao, M. Lu, X. M. Ding, X. Y. Hou, X. M. Zhang, X. Q. He, and S. T. Lee, Adv. Mater. **12**, 265 (2000).
[49] S. R. Forrest, P. E. Burrows, and M. E. Thompson, in *Organic Electroluminescent Materials and Devices* (Ref. 7), Chap. 13.
[50] L. S. Forster, Coord. Chem. Rev. **227**, 59 (2002).
[51] P. J. Hay, J. Phys. Chem. A **106**, 1634 (2002).